

Magnetic tornadoes and chromospheric swirls – Definition and classification.

Sven Wedemeyer¹, Eamon Scullion¹, Oskar Steiner², Jaime de la Cruz Rodriguez³ and Luc Rouppe van der Voort¹

¹ Institute of Theoretical Astrophysics, University of Oslo, P.O. Box 1029 Blindern, N-0315 Oslo, Norway

² Kiepenheuer Institute for Solar Physics, Schöneckstr. 6-7 D-79104 Freiburg, Germany

³ Department of Physics and Astronomy, Uppsala University, Box 516, SE-75120 Uppsala, Sweden

E-mail: sven.wedemeyer@astro.uio.no

Abstract. Chromospheric swirls are the observational signatures of rotating magnetic field structures in the solar atmosphere, also known as magnetic tornadoes. Swirls appear as dark rotating features in the core of the spectral line of singly ionized calcium at a wavelength of 854.2 nm. This signature can be very subtle and difficult to detect given the dynamic changes in the solar chromosphere. Important steps towards a systematic and objective detection method are the compilation and characterization of a statistically significant sample of observed and simulated chromospheric swirls. Here, we provide a more exact definition of the chromospheric swirl phenomenon and also present a first morphological classification of swirls with three types: (I) Ring, (II) Split, (III) Spiral. We also discuss the nature of the magnetic field structures connected to tornadoes and the influence of limited spatial resolution on the appearance of their photospheric footpoints.

1. Introduction

The combination of photospheric vortex flows and magnetic fields produces rotating magnetic field structures in the solar atmosphere, which are both seen in high-resolution observations and numerical simulations (Wedemeyer-Böhm et al. 2012, hereafter Paper I). The streamlines, which trace the simulated velocity field of the plasma in the rotating field structures, have a narrow footpoint in the photosphere, which broadens into a wide funnel in the chromosphere above (see Fig. 1). This appearance is reminiscent of tornadoes on Earth, which led to the name ‘magnetic tornadoes’ for this solar phenomenon. The term ‘tornado’ has already been used before for vertically aligned spiral structures in connection with prominences (see Chap. 10 by Tandberg-Hansen in Bruzek & Durrant 1977). Such ‘solar tornadoes’¹ were observed with the Coronal Diagnostic Spectrometer (CDS, Harrison et al. 1995) onboard the Solar and Heliospheric Observatory (SOHO, Domingo et al. 1995), implying that rotation may play an important role for the dynamics of the solar transition region (Pike & Harrison 1997; Pike & Mason 1998; Banerjee et al. 2000). More recent observations with the Solar Dynamics Observatory (SDO, Lemen et al. 2012) revealed more details of this phenomenon (Li et al. 2012).

¹ See the ESA press release at http://www.esa.int/esaCP/Pr_15_1998_i_EN.html

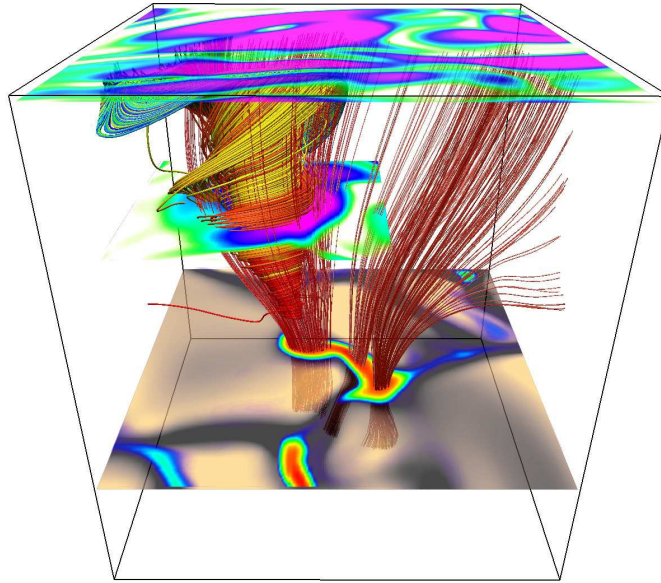


Figure 1. Visualization of a close-up region from the numerical simulation with a magnetic tornado. The red (mostly vertical) lines represent magnetic field lines, whereas the red/orange/yellow wound lines trace the velocity field in the tornado in this snapshot. The lower surface shows the granulation superposed with the absolute magnetic field strength at the bottom of the photosphere. The other layers show the horizontal velocity at heights of 1000 km and 2000 km with pink marking the highest speeds. Created with VAPOR (Clyne et al. 2007).

There is some indication that these giant tornadoes can be explained as rotating magnetic structures driven by underlying photospheric vortex flows just like the magnetic tornadoes described in Paper I (Su et al. 2012; Orozco Suárez et al. 2012). The connection between the prominence-related giant tornadoes and the smaller magnetic tornadoes is not clear yet. However, it is established that photospheric vortex flows, which are an essential ingredient of tornadoes, are a common phenomenon on the Sun. Vortex flows are seen both in observations (e.g. Brandt et al. 1988; Bonet et al. 2008, 2010; Steiner et al. 2010; Vargas Domínguez et al. 2011) and in numerical simulations (e.g. Nordlund 1985; Stein & Nordlund 1998; Vögler et al. 2005; Steiner et al. 2010; Kitiashvili et al. 2011; Shelyag et al. 2011; Moll et al. 2012, Paper I).

Here, we present a first definition and classification of chromospheric swirls (Wedemeyer-Böhm & Rouppe van der Voort 2009, hereafter Paper II), which is the essential observational signature of magnetic tornadoes, and address the appearance of the magnetic footpoints, which are another essential indicator of a magnetic tornado.

2. Numerical simulations

The analysis in Paper I was primarily based on numerical simulations with the 3-D radiation magnetohydrodynamics code CO⁵BOLD (Freytag et al. 2012; Wedemeyer et al. 2004). The computational box of these models has a horizontal size of 8 Mm \times 8 Mm and extends vertically from 2.4 Mm below the optical depth level $\tau_c = 1$ to 2.0 Mm above it, i.e., to the top of the chromosphere. The initial model was derived from a non-magnetic simulation, which was supplemented with an initially vertical, homogeneous magnetic field with a field strength of $B_0 = 50$ G. Periodic lateral boundaries and an open lower boundary were used, whereas the top boundary is transmitting for hydrodynamics and outward radiation. The tangential magnetic field component vanishes at the top boundary, i.e., there, the magnetic field is vertical.

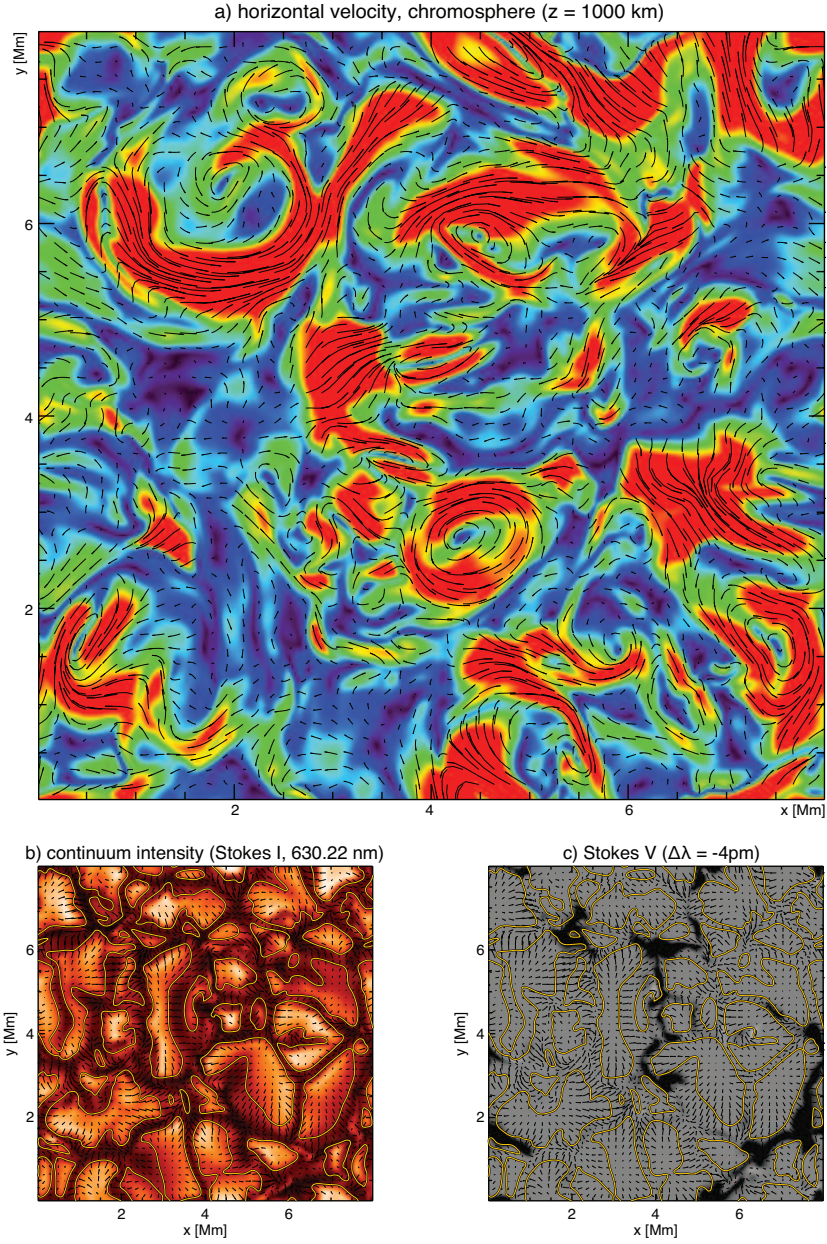


Figure 2. (a) Horizontal cross-section through a simulation snapshot at $z = 1000$ km (chromosphere) displaying in colors the absolute value of the horizontal velocity and the projected streamlines. (b) The corresponding continuum intensity (Stokes I at $\lambda = 630.22$ nm) and (c) Stokes V at $\Delta\lambda = -4$ pm from line center. The contours for $v_z = 0$ km/s in the lower panels outline the granule boundaries, while the streamlines trace the horizontal velocity field.

No artificial limiting of the Alfvén speed has been imposed. The analysis of the magnetic tornadoes in Paper I was done on a sequence with 1 s cadence. In Fig. 2, cross-sections through one of these snapshots are shown. The upper panel displays the (horizontal) flow pattern in the chromosphere. There are about a dozen chromospheric swirls of different types and sizes (some cases more obvious than others), indicating that swirl events are very common in the simulations. Typically, every second magnetic footpoint in the photosphere is connected to a swirl in the chromosphere above.

3. Magnetic tornadoes and chromospheric swirls – Definition and classification

3.1. Conditions for the formation of tornadoes

In the photosphere, the plasma flows away from the granule interiors and towards the intergranular lanes, where the cooled plasma shoots back down into the convection zone (see Fig. 2b). The flow carries a net angular momentum. Due to the conservation of angular momentum, the downflows in the lanes can create vortex flows (‘bathtub effect’, see, e.g., Nordlund 1985). Vortex flows are formed most easily at the vertices of lanes, where plasma meets from the neighbouring granules. The flows also advect magnetic field into the intergranular lanes, where the field is concentrated and thus amplified. Consequently, vortex flows and magnetic field concentrations often exist at the same locations. A stationary magnetic tornado is generated when the magnetic field concentration is perfectly co-located with the vortex flow, resulting in the rotation of the entire magnetic structure. However, exact co-location is not always perfectly fulfilled. A magnetic field structure can be partially pushed into a vortex and out again, which results in a partial rotation of the magnetic field structure but not in a stationary tornado. We therefore expect tornadoes to exhibit a spectrum of rotational behavior, from partial to stationary rotation.

3.2. Chromospheric swirls as observable signature of tornadoes

Swirls have been discovered as dark rings in the line core of the calcium infrared triplet line at a wavelength of 854.2 nm during an observation campaign at the Swedish 1-m Solar Telescope (SST) (Scharmer et al. 2003) in 2008 (Paper II). We refer to this observational imprint as the Ca line core signature (CLCS) or Ca 854 swirl hereafter. It is the only direct indicator of chromospheric swirls and magnetic tornadoes known so far. This is due to the fact that detecting swirls is a challenging task, which requires stable, high-quality image series with high spatial and temporal resolution for a purely chromospheric diagnostic. In this respect, a narrow wavelength transmission range is crucial because the subtle swirl signature is only visible if the intensity signal is not contaminated by large contributions from the line wings, which are formed lower in the atmosphere. The CRISP instrument (Scharmer et al. 2008) at the SST offers this possibility, but even with this instrument, the observation of chromospheric swirls is still challenging.

3.3. Definition – What is a chromospheric swirl?

In accordance with Paper II, we note that the swirl pattern can be seen as darkening in the Ca II 854.2 nm line core at wavelengths down to $\Delta\lambda \approx 70$ pm. The intensity at wavelengths further away from the line core originate from deeper down in the atmosphere, where the rotating magnetic structure has a smaller extent and is thus less clearly visible. There is a corresponding brightening with mostly the same pattern in the red line wing close to the line core, produced by the Doppler shift within the swirl. Based on these observations and supporting numerical simulations, we formulate the following conditions that need to be fulfilled for a chromospheric swirl:

- (i) Ca II 854 nm line core images exhibit a dark ring, a ring fragment or a spiral (see Fig. 3).
- (ii) The Ca 854 swirl is rotating.
- (iii) The Ca 854 swirl is visible for several minutes.
- (iv) Vertical velocities (Doppler-shifts at disk centre) on the order of at least 2 km/s and more can be measured at locations coinciding with the Ca 854 swirl.
- (v) A photospheric magnetic field concentration is visible at the same location, e.g., in the form of a magnetic bright point and/or in the magnetogram.

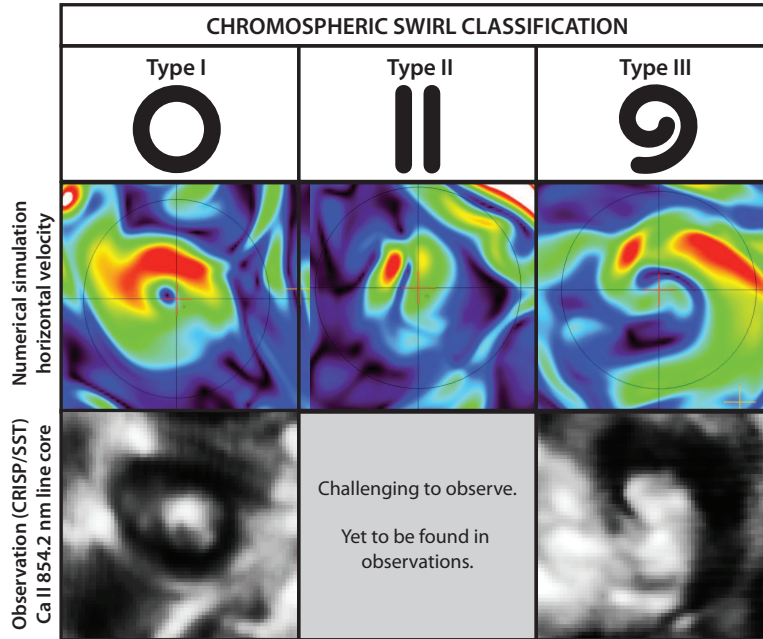


Figure 3. The three major types of chromospheric swirls: Type I (Ring), type II (Split), and type III (Spiral). The middle row shows the color-coded horizontal velocity in horizontal cross-sections at $z = 1000$ km for swirls in the numerical simulation (Paper I). Observed examples of type I and III swirls are presented in the bottom row. The images are taken in the line core of the Ca II infrared triplet line at 854.2 nm (Paper II).

3.4. Classification

Swirls can have different shapes in the Ca line core images as already stated in Paper II. The shapes are also seen in horizontal cross-sections of the horizontal velocity at chromospheric heights in the numerical models. The three most prominent types are shown in Fig. 3:

Type I:	Ring.	Example in Fig. 2a: [$x = 4.3$ Mm, $y = 2.7$ Mm]
Type II:	Split.	Example in Fig. 2a: [$x = 4.0$ Mm, $y = 4.6$ Mm]
Type III:	Spiral.	Example in Fig. 2a: [$x = 1.9$ Mm, $y = 6.4$ Mm]

All three types are seen in numerical simulations and types I and III are observed. A type I swirl is not necessarily a closed ring but can consist of ring fragments, too. Some simulation examples suggest that type I swirls can evolve into type II as the circular flow pattern becomes increasingly elongated until the swirl signature fades away. A type III swirl can also have multiple spiral arms. Based on a preliminary analysis of the simulations, half of the cases are classified as type I, and one fourth as type II and III, respectively. Type I swirls are possibly connected to open field structures, which can rotate more freely than the legs of closed loops. The latter build up more twist, which might result in spiral-like type III swirls.

4. Photospheric footpoints of magnetic tornadoes

The existence of a photospheric bright point as magnetic field indicator below a chromospheric swirl is a necessary condition for the detection of a magnetic tornado. However, the sizes of magnetic bright points (MBP) can be very small so that their identification and tracking over time is affected by the spatial resolution of the employed instrument. In the following, we discuss implications for the detection of tornado-related MBPs.

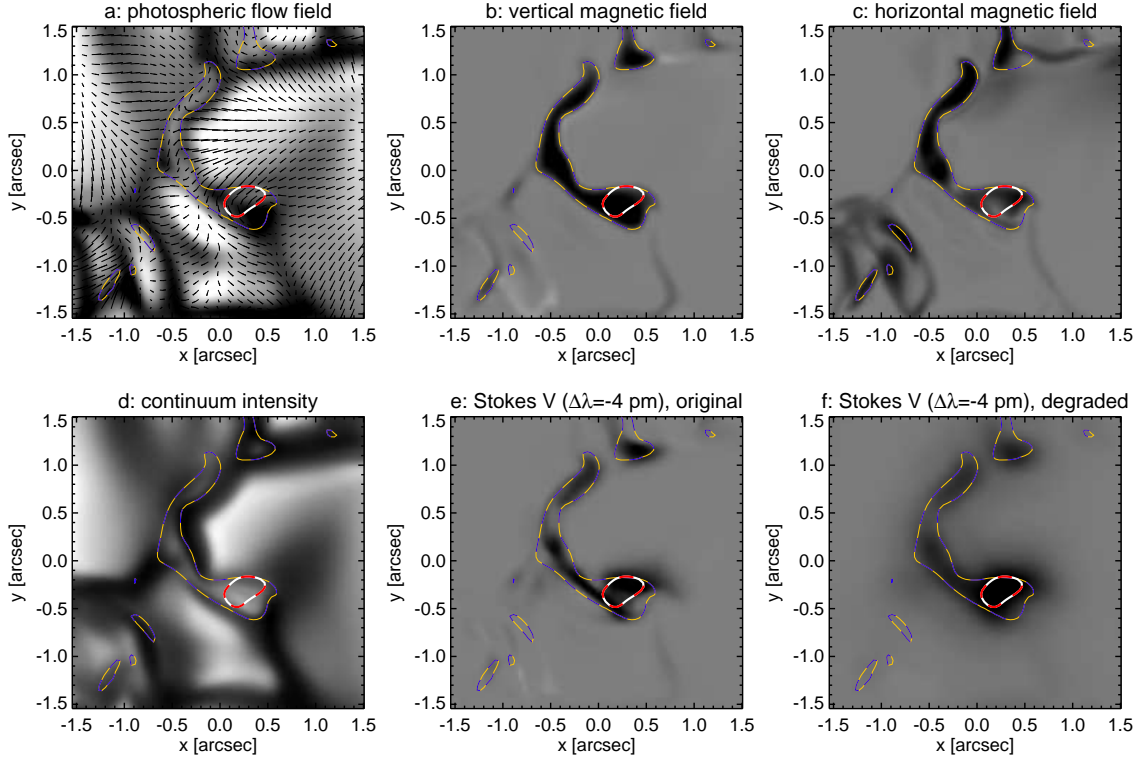


Figure 4. Effect of limited spatial resolution on the appearance of the magnetic flux topology shown for a small close-up region from a magnetohydrodynamical simulation (Fig. 2b-c, Paper I). **a)** Flow field at the bottom of the photosphere. The vertical velocity component is plotted in grey-scale, whereas the horizontal components in the plane are represented by arrows. **b)** The vertical magnetic field component and **c)** the horizontal magnetic field $((B_x^2 + B_y^2)^{1/2})$ in the same plane. **d)** The continuum intensity (Stokes I at a wavelength of $\lambda = 630.22$ nm). **e)** Original Stokes V map at $\Delta\lambda = -4$ pm from line center and **f)** the Stokes V map after a PSF has been applied. The blue-yellow dashed lines are contours of the absolute magnetic field strength at $|B| = 400$ G, whereas the red-white dashed contour outlines the magnetic concentration that is visible in the degraded image (f).

The magnetized plasma of the solar atmosphere – A continuous medium. Starting from the initial model, the magnetic field quickly concentrates in the vertices of intergranular lanes and a complex and entangled magnetic field structure evolves. It is possible to identify groups of magnetic field lines that rotate and/or sway together. These groups usually do not persist for long because the magnetic field is continuously rearranged on short time scales connected to the lifetime of granules and the resulting changes in the photospheric flow field. Like other authors before (e.g., Stein & Nordlund 2006), we argue that the appearance of flux tubes is (at least partially) the product of the limited spatial resolution of the observations, resulting in apparently separated MBPs. It would be more appropriate to talk of a continuous magneto-fluid in which the field lines at neighbouring locations exhibit similar dynamics, rather than to describe the magnetic field as individual, isolated flux tubes.

The effect of limited spatial resolution is illustrated in Fig. 4, which displays a close-up region in a numerical simulation snapshot (see Sect. 2). As result of the convective flows (Fig. 4a), the magnetic field is arranged in the form of continuous sheets and knots (see B_z in panel b and

$B_h = (B_x^2 + B_y^2)^{1/2}$ in panel c). The strongest field concentrations appear as bright features in the continuum intensity (panel d), although the correlation between magnetic field strength and intensity is not strict. The corresponding magnetogram for the Fe I line at a wavelength of 630.2 nm is shown in panel e. This magnetogram, i.e., the Stokes V signal, is calculated with the full-Stokes radiative transfer code NICOLE (Socas-Navarro 2011; de la Cruz Rodríguez et al. 2012) along vertical lines of sight. The Stokes signal is formed over a height range in the atmosphere, whereas the magnetic field in panels b and c refers to a single horizontal cross-section at the bottom of the photosphere only. The resulting magnetogram appears therefore more intermittent and less continuous than the magnetic field in the horizontal plane. Next, the magnetogram is convolved with a point spread function (PSF, see Wedemeyer-Böhm 2008) that simulates the effect of a telescope with an aperture of 50 cm, which is equivalent to the Solar Optical Telescope (SOT, Tsuneta et al. 2008; Suematsu et al. 2008; Ichimoto et al. 2008; Shimizu et al. 2008) onboard the Hinode spacecraft (Kosugi et al. 2007). The resulting degraded magnetogram is shown in Fig. 4f. It should be noted that this degradation is optimistic. In practice, the derivation of the Stokes components from measurements with limited spatial, temporal, and spectral resolution would result in magnetograms that are even more diffuse and less reliable than the synthetic example presented here. Nevertheless, the effect of the limited spatial resolution is obvious. Only individual blobs of enhanced Stokes V signal remain instead of the continuous magnetic flux sheet in the original model atmosphere. When observed, these blobs would be identified as MBPs. The most prominent MBP is outlined with a red-white dashed contour in Fig. 4. Most of the remaining magnetic field (blue-yellow contours) would remain undetected. In particular, the thin magnetic flux sheets in the intergranular lanes are barely visible. In view of this effect, the question arises how uniquely a MBP can be identified. During an observation run, a MBP can be tracked from its first appearance until its disappearance as long as it remains sufficiently separated from other MBPs. In that case a lifetime can be determined. However, the numerical simulations suggest that the magnetic field is continuously reorganised. Some of the magnetic field, which would be observed as part of the MBP, may be advected into a neighbouring sheet and, in return, additional field may be advected into the MBP. These changes would remain undetected, whereas the same MBP appears to persist. The lifetimes of observed MBPs are consistent with the timescales on which the granulation pattern evolves (e.g., Jafarzadeh et al. 2013, and references therein) but the magnetic field (incl. individual MBPs) can nevertheless last beyond the lifetime of the surrounding granules.

5. Discussion and Conclusions

The primary way to detect a chromospheric swirl and thus a magnetic tornado is the Ca II 854.2 nm line core signature (CLCS) so far, which requires a narrow filter transmission range. These requirements make it challenging to observe chromospheric swirls and, to our knowledge, only CRISP/SST observations have repeatedly produced successful swirl detections so far. Ultimately, more observations, preferably with a variety of instruments, are needed in order to gather a statistically significant sample that allows for a detailed characterization of magnetic tornadoes, including their occurrence, distribution of sizes and lifetimes and the related energy transport rates. These small-scale events represent a challenging test for the next generation of solar telescopes like ATST (Keil et al. 2011) and EST (Collados et al. 2010). High spatial resolution is not only important for the observations but also for the numerical simulations. The successful modelling of magnetic tornadoes requires the sufficient resolution of the narrow intergranular lanes, where photospheric vortex flows and magnetic fields coalesce.

Acknowledgments

SW thanks the organizers of the conference “Eclipse on the Coral Sea: Cycle 24 Ascending” GONG 2012/LWS/SDO-5/SOHO 27, which has been held in Palm Cove, Australia, in 2012.

References

- Banerjee, D., O'Shea, E., & Doyle, J. G. 2000, *A&A*, 355, 1152
- Bonet, J. A., Márquez, I., Sánchez Almeida, J., Cabello, I., & Domingo, V. 2008, *ApJ*, 687, L131
- Bonet, J. A., Márquez, I., Sánchez Almeida, J., et al. 2010, *ApJ*, 723, L139
- Brandt, P. N., Scharmer, G. B., Ferguson, S., Shine, R. A., & Tarbell, T. D. 1988, *Nature*, 335, 238
- Bruzek, A. & Durrant, C. J., eds. 1977, *Astrophysics and Space Science Library*, Vol. 69, Illustrated glossary for solar and solar-terrestrial physics
- Clyne, J., Mininni, P., Norton, A., & Rast, M. 2007, *New J. Phys*, 9, 1
- Collados, M., Bettonvil, F., Cavaller, L., et al. 2010, *Astronomische Nachrichten*, 331, 615
- de la Cruz Rodríguez, J., Socas-Navarro, H., Carlsson, M., & Leenaarts, J. 2012, *A&A*, 543, A34
- Domingo, V., Fleck, B., & Poland, A. I. 1995, *Sol. Phys.*, 162, 1
- Freytag, B., Steffen, M., Ludwig, H.-G., et al. 2012, *Journal of Computational Physics*, 231, 919
- Harrison, R. A., Sawyer, E. C., Carter, M. K., et al. 1995, *Sol. Phys.*, 162, 233
- Ichimoto, K., Katsukawa, Y., Tarbell, T., et al. 2008, in *Astronomical Society of the Pacific Conference Series*, Vol. 397, *First Results From Hinode*, ed. S. A. Matthews, J. M. Davis, & L. K. Harra, 5
- Jafarzadeh, S., Solanki, S. K., Feller, A., et al. 2013, *A&A*, 549, A116
- Keil, S. L., Rimmele, T. R., Wagner, J., Elmore, D., & ATST Team. 2011, in *Astronomical Society of the Pacific Conference Series*, Vol. 437, *Solar Polarization 6*, ed. J. R. Kuhn, D. M. Harrington, H. Lin, S. V. Berdyugina, J. Trujillo-Bueno, S. L. Keil, & T. Rimmele, 319
- Kitiashvili, I. N., Kosovichev, A. G., Mansour, N. N., & Wray, A. A. 2011, *ApJ*, 727, L50
- Kosugi, T., Matsuzaki, K., Sakao, T., et al. 2007, *Sol. Phys.*, 243, 3
- Lemen, J. R., Title, A. M., Akin, D. J., et al. 2012, *Sol. Phys.*, 275, 17
- Li, X., Morgan, H., Leonard, D., & Jeska, L. 2012, *ApJ*, 752, L22
- Moll, R., Cameron, R. H., & Schüssler, M. 2012, *A&A*, 541, A68
- Nordlund, A. 1985, *Sol. Phys.*, 100, 209
- Orozco Suárez, D., Asensio Ramos, A., & Trujillo Bueno, J. 2012, *ApJ*, 761, L25
- Pike, C. D. & Harrison, R. A. 1997, *Sol. Phys.*, 175, 457
- Pike, C. D. & Mason, H. E. 1998, *Sol. Phys.*, 182, 333
- Scharmer, G. B., Bjelksjo, K., Korhonen, T. K., Lindberg, B., & Petterson, B. 2003, in *Society of Photo-Optical Instrumentation Engineers (SPIE) Conference Series*, ed. S. L. Keil & S. V. Avakyan, Vol. 4853, 341
- Scharmer, G. B., Narayan, G., Hillberg, T., et al. 2008, *ApJ*, 689, L69
- Shelyag, S., Keys, P., Mathioudakis, M., & Keenan, F. P. 2011, *A&A*, 526, A5
- Shimizu, T., Nagata, S., Tsuneta, S., et al. 2008, *Sol. Phys.*, 249, 221
- Socas-Navarro, H. 2011, *A&A*, 529, A37
- Stein, R. F. & Nordlund, A. 1998, *ApJ*, 499, 914
- Stein, R. F. & Nordlund, Å. 2006, *ApJ*, 642, 1246
- Steiner, O., Franz, M., Bello González, N., et al. 2010, *ApJ*, 723, L180
- Su, Y., Wang, T., Veronig, A., Temmer, M., & Gan, W. 2012, *ApJ*, 756, L41
- Suematsu, Y., Tsuneta, S., Ichimoto, K., et al. 2008, *Sol. Phys.*, 249, 197
- Tsuneta, S., Ichimoto, K., Katsukawa, Y., et al. 2008, *Sol. Phys.*, 249, 167
- Vargas Domínguez, S., Palacios, J., Balmaceda, L., Cabello, I., & Domingo, V. 2011, *MNRAS*, 416, 148
- Vögler, A., Shelyag, S., Schüssler, M., et al. 2005, *A&A*, 429, 335
- Wedemeyer, S., Freytag, B., Steffen, M., Ludwig, H.-G., & Holweger, H. 2004, *A&A*, 414, 1121
- Wedemeyer-Böhm, S. 2008, *A&A*, 487, 399
- Wedemeyer-Böhm, S. & Rouppe van der Voort, L. 2009, *A&A*, 507, L9 (Paper II)
- Wedemeyer-Böhm, S., Scullion, E., Steiner, O., et al. 2012, *Nature*, 486, 505 (Paper I)